IEEE Access
Multidisciplinary | Rapid Review | Open Access Journal

Received November 16, 2021, accepted December 4, 2021, date of publication December 27, 2021,
date of current version January 4, 2022.

Digital Object Identifier 10.1109/ACCESS.2021.3138890

Built-in Sensor System for Monitoring Internal Shear Strain and Stress Distribution in Soft Materials

FENGYU LI[1], YASUHIRO AKIYAMA[1], (Member, IEEE), XIANGLONG WAN[2], (Member, IEEE), SHOGO OKAMOTO[3], (Member, IEEE), AND YOJI YAMADA[1], (Member, IEEE)

[1]Department of Mechanical Systems Engineering, Graduate School of Engineering, Nagoya University, Nagoya 464-8603, Japan
[2]School of Automation and Electrical Engineering, University of Science and Technology Beijing, Beijing 100083, China
[3]Department of Computer Science, Graduate School of Systems Design, Tokyo Metropolitan University, Tokyo 192-0397, Japan

Corresponding author: Fengyu Li (li.fengyu@k.mbox.nagoya-u.ac.jp)

This work was supported by the Grants-in-Aid for Scientific Research (KAKENHI) of the Japan Society for the Promotion of Science under Grant 16H03134.

ABSTRACT Soft robotics require flexible sensors that can realize sensitive measurements for which rigid sensors are not viable. Precise and quantitative measurement of the mechanical phenomena is necessary in all the sensors; however, in the field of soft robotics, the complex structure and physical properties of composite materials complicate the construction of a precise sensing model. In this study, a built-in sensor system for internal shear strain and stress distribution measurement is developed by embedding piezoelectric polyvinylidene fluoride polymer films within the objective soft material. Shear-strain sensing models are established by relating the piezoelectricity and cantilever bending mechanics. For validation, experiments are conducted in which the deflection of the embedded film sensors is monitored and digitized using a video camera. The shear-strain sensing model is validated by evaluating the agreement between the modeled and measured physical variations, and a high coefficient of determination of 0.974 is obtained. In addition, based on the linear relation of the arithmetic expression of each sensing model, calibrated results for internal shear strain and stress sensing are successfully obtained. Furthermore, the measurement effect of this type of flexible sensor and its potential applications are discussed.

INDEX TERMS Built-in flexible sensor, multilayer elastic material, PVDF polymer film, shear strain distribution, soft robotics.

I. INTRODUCTION

Research on elastomeric and soft robotics has been extensive and significant in a wide range of areas, such as safe wearable soft sensors [1] and soft-bodied robots [2]. The flexibility of soft robotics allows them to be applied to unique cases, where rigid robots are not a viable option. In addition, they are safer for human interaction and internal deployment within the human body. Drastic changes in the shape and size are possible for adapting to various environments. Technological advancements have enabled the usage of such sensors in vital applications, such as in wearable assistive healthcare devices [1], [3], medical robotics [4], [5], and tactile sensors [6], [7].

In the field of stress and strain measurement, internal physical measurements are a well-known topic. Electrical strain gauges and optical strain sensors are generally applied for concrete structures [8]. However, for soft materials with high elasticity or viscoelasticity, direct measurement methods are rare. The general use of ultrasound images [9], [10] or tomographic particle image velocimetry [11] to monitor internal tissue displacement involves limited measurement environments and optical devices. Moreover, the realization of stringent and real-time measurement is difficult.

To solve this problem, sensitized electronic skin is used to synthesize the soft-substrate and built-in sensors [12]–[14]. Research on the installation of conventional transducers within the objective material has been limited owing to challenges in the architecture, manufacturing technology architecture, and manufacturing technology, and the difficulties in guaranteeing measurement accuracy [15].

Additionally, soft materials such as skin tissue are multilayered complex structures with different characteristics for each layer [16]. As the trend of reproducing the mechanical

The associate editor coordinating the review of this manuscript and approving it for publication was Laxmisha Rai.

characteristics of human skin has also facilitated the improvement of artificial skin [17], the study of sensor development will not be limited to homogeneous materials alone. The properties of the composite materials in embedded or multilayered structures should be carefully considered [18]. Most of the proposed soft sensing techniques have been tested only through simulation and are not yet ready for practical use. The improvement of soft sensors from the simulation stage to practical use is a significant challenge because the actual process dynamics are more complicated than the conditions considered in simulation experiments [19]. Therefore, to provide a more precise explanation of the proposed sensor system, the sensing model should be fully considered and validated.

In a previous study, Li *et al.* had developed a sensor system for measuring the internal shear strain distribution in soft materials by embedding an array of polyvinylidene fluoride (PVDF) films [20], [21]. PVDF, which is a thin film-type piezoelectric polymer [22], has attracted considerable interest because of its enhanced mechanical and thermal strength and piezoelectric properties [23]. In the field of robotics, it has been applied for pressure measurement [24], motion and vibration monitoring [25], [26], and slip detection for robot hand grasping [27]. The high mechanical flexibility of PVDF film sensors renders them suitable for establishing a soft-material built-in sensor system.

In this study, to realize the internal measurement of the shear strain and shear stress distribution in soft materials, a flexible PVDF film sensor is built in a bilayer substrate. Sensing models are proposed and validated through experiments in which the charge output and deflection of the embedded sensors are monitored through a transparent material. To clarify the sensing mechanism, the relation between the charge generation of the sensor and the deflection is mathematically presented, based on the piezoelectricity and the mechanics of the composite structure. Moreover, an artificial skin substrate with a bilayer structure is developed to tentatively observe the possible application of the sensor system to more complex structures.

II. SENSOR STRUCTURE AND SENSING MODELS

A. STRUCTURE OF THE EMBEDDED SENSOR SYSTEM

The uniqueness of the proposed sensor system is that the sensing elements are structured within the substrate soft material as an integrated system. The embedded flexible PVDF films are expected to reflect the mechanical properties of the deformed soft substrate material. In this study, the shear direction is set to take advantage of the high flexibility of the PVDF film. To improve the shear strain and stress component measurements, as illustrated in Fig. 1, the PVDF polymer films were fixed perpendicularly to the surface in the initial state. The physical variations in the soft material can be explained by the output charge induced through piezoelectricity. To measure the distribution, different embedded lengths of sensor elements were arranged in the depth direction at a position.

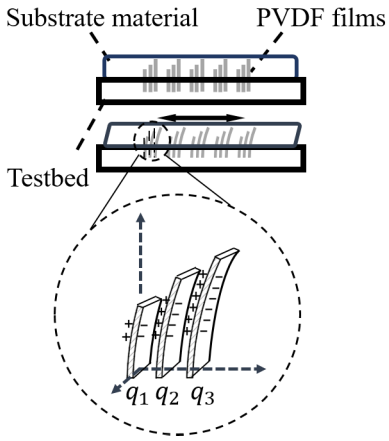

FIGURE 1. Schematic of the sensor system structure.

B. SHEAR STRAIN SENSING MODEL

The relationship between the output electrical charge from the PVDF polymer films and the physical information of the substrate material is mathematically described in order to explain the shear sensing mechanism. The measurement function is divided into shear strain and shear stress sensing models. The shear strain sensing model is first introduced. For perpendicularly embedded film sensors under shear deformation of the substrate, the deformation includes bending motion in the poling direction and stretching motion in the longitudinal direction. Therefore, the output of the PVDF sensor q_c during measurement is the combined result of the bending effect q_b and stretching effect q_s as follows:

$$q_c = q_b + q_s. \tag{1}$$

Each sensing model is explained below.

1) BENDING MODEL

A bending model was established based on the piezoelectricity and mechanical behavior of a bending cantilever beam. The charge generation under deflection of the PVDF film was calculated based on two main constitutive equations: the direct piezoelectricity equation of the PVDF and the bending curvature differential equation. According to the constitutive governing equation of piezoelectricity for sheet PVDF [28], the accumulated electric charge q_b induced by bending motion can be calculated as

$$q_b = e_{31} \int_{A_3} S_1 \, dA_3 \,, \tag{2}$$

where e_{31} is the piezoelectric coefficient (75 mC/m^2, measured using the forced oscillation technique and resonance method), S_1 is the bending strain, and A_3 is the electrode area of the PVDF surface. Subscripts 1 and 3 indicate the longitudinal direction and poling direction, respectively, corresponding to the l and n axes defined in Fig. 2. To obtain the expression for the bending strain S_1 of a cantilever beam from the curvature differential equation, the geometric deflection of the cantilever-based PVDF film in the $O - ln$ coordinate is shown schematically in Fig. 2. The origin O was set at the

midpoint of the fixed end. The l axis is in the longitudinal direction of the neutral surface in the undeformed configuration, whereas the m axis is in the plane of the structure perpendicular to the l axis. The bending strain is expressed in terms of the geometric dimension and deflection as follows [29]:

$$S_1(l) = -\frac{k \cdot h_c}{\rho(l)} = -k_h \frac{n''}{\left[1 + (n')^2\right]^{\frac{3}{2}}}, \tag{3}$$

where ρ is the curvature radius of the neutral layer, h_c is the distance from the center of the PVDF layer to the neutral axis, k_h is the coefficient of dimension revised by the correction factor k, and n is the deflection of the cantilever beam at any section in terms of l. n' and n'' represent the first and second derivatives of the deflected shape with respect to l, respectively.

Substituting S_1 with equation (3), the charge generation in (2) can be expressed as follows:

$$q_b = -k_h \cdot e_{31} \cdot b \int_0^L \frac{n''}{\left[1 + (n')^2\right]^{\frac{3}{2}}} dl, \tag{4}$$

establishing the relation between the charge and geometric deflection. The range of integration is the length from the root to the free-tip of the sensor film. L is the entire length of the sensor in the longitudinal direction.

The integral part of equation (4) is evaluated as follows:

$$\begin{aligned} q_b &= -k_h \cdot e_{31} \cdot b_p \int_{n'(0)}^{n'(L)} \frac{1}{\left[1 + (n')^2\right]^{\frac{3}{2}}} dn' \\ &= -k_h \cdot e_{31} \cdot b_p \frac{n'}{\sqrt{1 + (n')^2}} \Bigg|_{n'(0)}^{n'(L)} \end{aligned} \tag{5}$$

As the PVDF film sensor is perpendicularly fixed, the angle of deflection at the origin position is zero. The output charge generated by the PVDF film corresponds only to the gradient of the tip of the free-end of the film $n'(L)$, as follows:

$$q_b = -e_{31} \cdot k_h \cdot b_p \frac{n'(L)}{\sqrt{1 + [n'(L)]^2}}. \tag{6}$$

Therefore, $n'(L)$ can be expressed as

$$n'(L) = \frac{q_b}{\sqrt{(e_{31} k_h b_p)^2 - q_b^2}}. \tag{7}$$

According to the properties of the sensor system, the deflection $n(l)$ of the PVDF film is assumed to coincide with the internal deformation of the soft substrate. Therefore, $n'(L)$ represents the shear strain of the substrate at the tip of the free-end of the PVDF film. A series of mathematical equations for the piezoelectric-polymer-film bending motion can explain the application of this sensor system for shear strain monitoring.

Additionally, a remaining parameter that must be determined is k_h in equation (6), as shown in Fig.2. This is the dimensional coefficient of the PVDF sensor and is a constant.

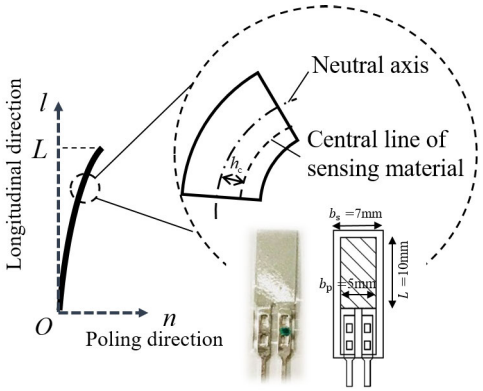

FIGURE 2. Orientation and geometric deflection of the PVDF polymer film.

For the q_b model, equation (6) can be factored as two parts: constant parameters and geometrical terms.

$$q_b = K \cdot H, \tag{8}$$

where

$$K = e_{31} \cdot k_h \cdot b_p, \tag{9}$$

and

$$H = -\frac{n'}{\sqrt{1 + (n')^2}} \Bigg|_{n'(0)}^{n'(L)}. \tag{10}$$

The constant parameter K, including k_h, can be calibrated based on the proportional relation of the charge generation q_b and geometrical term H.

2) STRETCHING MODEL

The composite structure necessitates the consideration of the interaction between the embedded sensor element and the substrate in the sensing mechanism. Because built-in films do not perfectly follow the deformation of the substrate and a stretching press occurs in the longitudinal direction under shear deformation, a stretching model is additionally combined with the sensing model. The stress effect along the longitudinal direction of the sensor is defined as τ_1, and depicted in Fig. 3.

The small triangle in the figure represents a unit in the elastic substrate used to calculate the interface press of σ_3 and τ_1. σ_3 on the two sides of the film is considered to be in equilibrium and does not apply an additional press in the poling direction. Therefore, the charge q_s, which is affected by the surrounding stress distribution, can be expressed as

$$\begin{aligned} q_s &= d_{31} \int_A \tau_1 dA \\ &= d_{31} \cdot b_p \int_0^L \tau_1 dl, \end{aligned} \tag{11}$$

$$\tau_1 = \tau_{xz} \left(\sin^2\theta - \cos^2\theta\right) + (\sigma_z - \sigma_x) \sin\theta \cos\theta, \tag{12}$$

$$\theta = \arctan\left(\frac{dl}{dn}\right) = \operatorname{arccot}\left(n'\right), \tag{13}$$

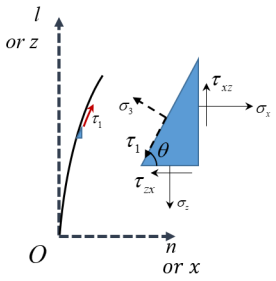

FIGURE 3. Schematic illustration of the stress effect from the substrate to the film sensor.

where d_{31} is the piezoelectric coefficient with a value of 25 pC/N, which is also measured using the forced oscillation technique and resonance method.

Because there is no direct measurement method to obtain the internal stress, the modeling function must be expressed using deformation variables. The stress components were transformed into a strain expression using Hook's law as follows:

$$\begin{aligned} \sigma_x &= 2G\varepsilon_x + \lambda\left(\varepsilon_x + \varepsilon_z\right) \\ \sigma_z &= 2G\varepsilon_z + \lambda\left(\varepsilon_x + \varepsilon_z\right) \\ \tau_{xz} &= G\gamma_{xz}, \end{aligned} \tag{14}$$

where G is the shear modulus of the substrate. Thus, τ_1 in equation (11) can be expressed using deformation parameters alone:

$$\begin{aligned} \tau_1 &= G\gamma_{xz}\left(\sin^2\theta - \cos^2\theta\right) + 2G\left(\varepsilon_z - \varepsilon_x\right)\sin\theta\cos\theta \\ &= G\left[\left(\varepsilon_y - \varepsilon_x\right)\sin 2\theta - \gamma_{xz}\cos 2\theta\right] \\ &= G\left[\left(\frac{\partial v}{\partial z} - \frac{\partial u}{\partial x}\right)\sin 2\theta - \left(\frac{\partial u}{\partial z} - \frac{\partial v}{\partial x}\right)\cos 2\theta\right]. \end{aligned} \tag{15}$$

C. SHEAR STRESS SENSING MODEL

Another measurement function is the shear stress sensing mode. The shear stress can be directly obtained from the result of the shear strain model if the physical characteristics of the applied substrate material have been preliminarily obtained. Based on the mechanics of the materials, the shear stress component τ_{xz} is calculated by multiplying the shear strain γ_{xz} with the shear modulus G of the local substrate material using the following equation:

$$\tau_{xz} = G \cdot \gamma_{xz}. \tag{16}$$

However, as an integrated system, the composite material of the substrate material as well as the embedded sensor elements should be considered to clarify the mechanical properties. Although it is assumed that the highly flexible film sensor element complies with the deformation of the substrate, as a discontinuous material, new variables need to be defined for the composite material.

As illustrated in Fig. 4, the measurement position, which is the tip of the free-end of the film, is the focused upon. The deformed material unit is extracted as a composite material

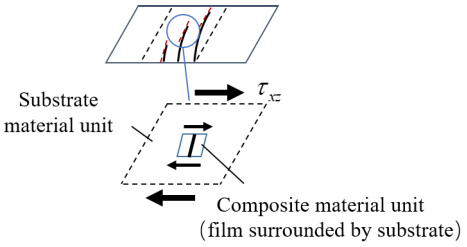

FIGURE 4. Composite material unit composed of sensor film and substrate.

unit, whose mechanical properties are determined by both the substrate and sensor stiffness. The shear modulus is defined as G_{com} . This inherent property parameter is generally calibrated before measurement using a series of stress-strain data. Under simple shear deformation, the shear strain γ_{xz} is obtained based on the previous shear strain model. Shear stress τ_{xz} can be applied as the surface shear stress because it is translated evenly within the sensor system in the depth direction [30].

In addition, when the shear deformation induced from the surface is in displacement control, shear stress τ_{xz} is transformed from the surface displacement X as follows:

$$\tau_{xz} = G \cdot \frac{X}{h}, \tag{17}$$

where h is the thickness of a single layer of the substrate. As mentioned in the introduction, this study uses a substrate with two material layers, leading to the following transformation:

$$\begin{aligned} \tau_{xz} &= G_i \cdot \gamma_i \\ &\sum_{i=1}^{2} h_i \cdot \gamma_i = X, \end{aligned} \tag{18}$$

where subscript i refers to each layer.

In consequence, the shear stress sensing model is given as

$$\tau_{xz} = \frac{G_1 \cdot X}{G_2 \cdot h_1 + G_1 \cdot h_2} = G_{\text{com}} \cdot \gamma_{xz}. \tag{19}$$

III. EXPERIMENT AND DATA PROCESSING METHOD

A. EXPERIMENTAL SETUP

Experiments were conducted to validate the sensing models of the proposed sensor system and clarify the measurement effect. For sensor testing, as depicted in Fig. 5, a bilayer structure with two types of artificial skin (HITOHADA GEL, EXSEAL Co., Ltd., Mino, Japan) is utilized as the soft substrate material. The upper-layer (blue colored) has an ASKER-C hardness of seven, whereas the lower layer (yellow colored) has an ASKER-C hardness of zero; the shear moduli of the upper and lower layers are 1.35×10^5 and 0.54×10^5 Pa, respectively. Thicknesses h_1 and h_2 shown in equation(19) are both 6 mm. Within the bilayer substrate, six PVDF films (KUREHA Co.,Ltd, Japan) are arranged at the central position beneath the substrate material without the influence of the periphery. The six PVDF films are aligned and embedded at various depths, corresponding to measured

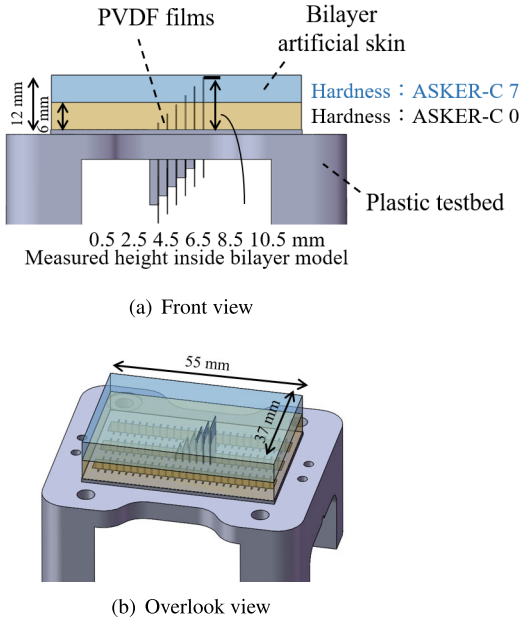

FIGURE 5. PVDF arrangement in the bilayer model.

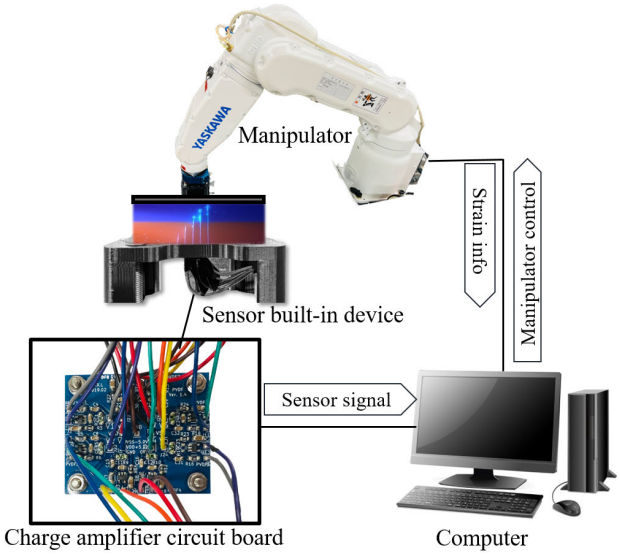

FIGURE 6. Experimental system [20].

heights of 0.5, 2.5, 4.5, 6.5, 8.5, and 10.5 mm, respectively, from left-to-right. The measured height refers to the length of the free-end of the sensor from a fixed position, as explained in the sensing model.

A plastic testbed with inlaid clamps matching the film thickness was manufactured as a PVDF film supporter using a three-dimensional printer. For signal transmission, electric wiring from the solder tabs was performed below the testbed.

The experimental setup is shown in Fig. 6. External stress was applied using a manipulator (MOTOMAN-MH5F, Yaskawa Electric Co., Ltd., Kitakyushu, Japan). Dynamic simple shear deformation was provided by a 2-Hz sinusoidal waveform in the horizontal direction. The low-frequency region was focused upon because investigation of skin contact safety showed that the frequency range of skin vibration was up to 10-Hz [31]. The part that contacted the substrate surface was designed as a large, square acrylic board to cover the entire device. Note that the contact part did not slip on the substrate, and the surface motion strictly agreed with the contact plate. A signal conditioning method was developed using a suitable charge amplifier circuit to achieve a real-time charge output with high signal-to-noise ratio [20]. The amplifier provided stable signal amplification in a wide frequency range up to 100-Hz such that the influence of the phase shift induced by vibration could be neglected.

1) SHEAR STRAIN MODEL VALIDATION TEST

The shear strain sensing model was validated by comparing the calculated result with the measured charge generation. Calculation of q_b and q_s according to equations (6)–(11) requires the measurement of the film sensor deflection. Taking advantage of the transparent substrate material, the embedded sensor wass clearly filmed using a video camera from the lateral-side. The shear deformation condition with a surface displacement amplitude of 2.5 mm was selected as the analysis target.

To capture the quantitative position $n - l$ of the films in the coordination, the images recorded by the video camera were processed. Pictures of the film deflection under maximum shear deformation were extracted using GetData Graph Digitizer(Version 2.26.0.20, S. Fedorov, Russia), as shown in Fig. 7a. The lines of the film profile were then extracted in the defined coordinate, and the deflection was digitized. Further, the curves were fitted to each series of points through polynomial curve fitting. The polynomial degree was set to three and six for the three shorter and longer films each, respectively, because the longer one had more complex deflection. Finally, the specific information of the optimized film curve can be obtained, as shown in Fig. 7b. Therefore, the modeled charge generation q_c, including q_b and q_s, can be calculated from the deflection data.

Note that the initial state of the film might not be perfectly vertical to the horizontal line. The variation in deflection is defined based on the initial arrangement condition of each sensor film. Moreover, the calibration result K was obtained from the proportional relation of q_b and the geometric term according to equations (13).

2) SHEAR STRESS MODEL VALIDATION TEST

Sequentially, the function of the shear stress sensing model was tested based on equation (19). To validate the linear relation between the shear stress and strain, a series of data were measured under different shear deformation amplitudes A from 0.5–5.5 mm. The shear stress τ_{xz} was obtained by substituting X with A according to the left-side of equation (19), and the shear strain γ_{xz} was obtained by substituting the measured charge in the strain-sensing model.

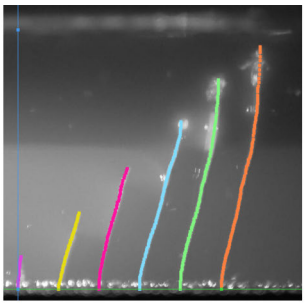

(a) Film deflection digitization.

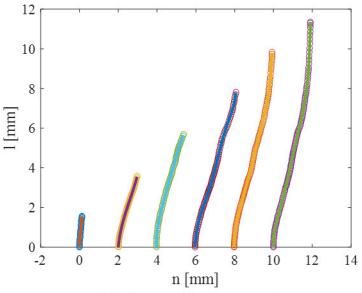

(b) Curve fitting result.

FIGURE 7. Film deflection in the defined coordinate.

IV. RESULT

A. VALIDATION RESULT OF THE SHEAR STRAIN SENSING MODEL

The modeled charge generation of the PVDF was compared with the directly measured charge output to validate the established shear strain sensing model. Fig. 8 shows the measured charge generation amplitude distribution q_{m} from each sensor for 15 measurement trials. The horizontal axis is the embedded length of the sensing area L of six sensors. Under sinusoidally varied shear deformation, the results of the maximum deformation states in two opposite directions are plotted in the same figure. To better observe the symmetry, the vertical axis (orange colored) denoting the negative output under the minus shear direction is reversed. Both results present an inflection in the distribution tendency at the interlamination boundary, which is marked by a broken line. The output signal initially increases from the bottom in the softer layer and then decreases incessantly up to the contact surface. The output between the two shear directions shows an approximately symmetrical distribution.

Further, using the digitized deflection of each PVDF film, the modeled charge from the bending model q_{b} and stretching model q_{s} is obtained; however, compared to the measured output result q_{m}, the result of the stretching model q_{s} is more than two orders of magnitude smaller. Hence, for shear strain sensing, the bending model is sufficiently sensitive to represent the mechanism.

For calibration, Fig. 9 plots the linear relation of geometric term H and q_{b} according to equations (8)–(10). The vertical axis q_{b} is obtained by subtracting the measured result on stretching the model part, $q_{\mathrm{m}} - q_{\mathrm{s}}$. The constant parameter represented by K is summarized from the slope as 783.57.

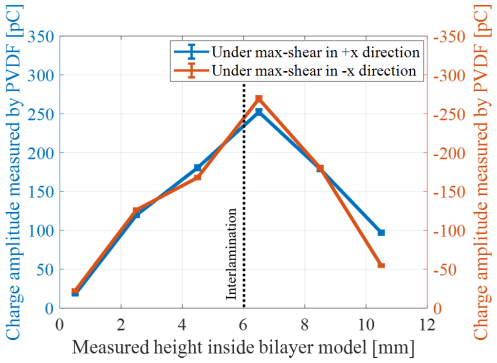

FIGURE 8. Charge output amplitude distribution measurement result from each sensor.

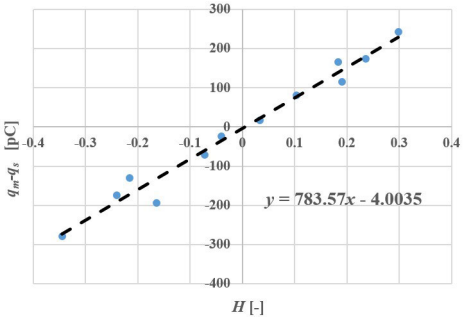

FIGURE 9. Proportional relation to summarize coefficient K.

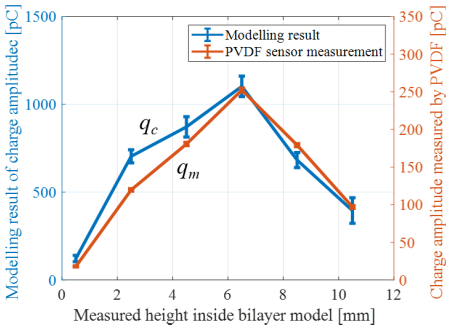

(a) Under maximum deformation in the $+x$ axis

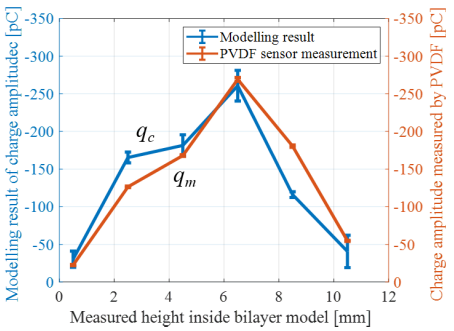

(b) Under maximum deformation in the $-x$ axis

FIGURE 10. PVDF arrangement in the bilayer model.

The modeling result q_{c} from equation (1) is compared with the measurement result q_{m} under the maximum deformation in Fig. 10. The results under each of the two shear directions

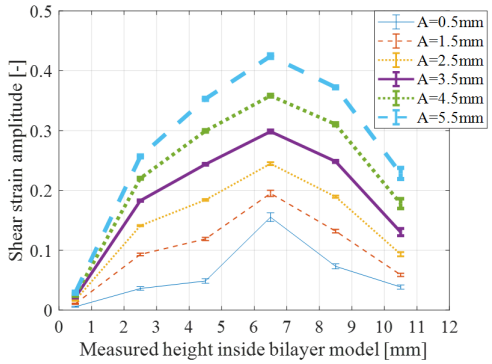

FIGURE 11. Measured local shear strain result at different deformations under 2 Hz.

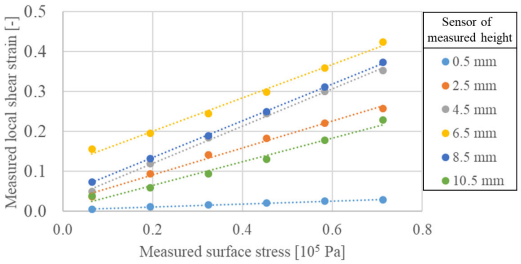

FIGURE 12. Linear relation to obtain the composite shear modulus.

are plotted. The twelve pairs of results from six PVDF films in Fig. 10 were used to reach an agreement. The agreement of q_c and q_m is evaluated based on the coefficient of determination $R^2 = 0.974$, indicating the significance of the prediction of the established model. Furthermore, the root mean squared error in 26.06 pC and the mean absolute percentage error of 19.8% of q_c based on q_m additionally confirm the excellent agreement.

B. VALIDATION RESULT OF THE SHEAR STRESS SENSING MODEL

The linear relation between the shear stress conditions and the measured strain was evaluated to validate the established shear stress model. Fig. 11 shows the measured shear strain distributions of the six PVDF films. The different strain distribution lines correspond to different maximum deformations A.

Further, using the above data, the relationship between the shear strain γ_{xz} of each PVDF film and the corresponding shear stress τ_{xz} is plotted in Fig. 12. The different lines correspond to different PVDF films. The linear variation validates the shear stress sensing model, and the reciprocal slope of the regression line represents the composite shear modulus G_{com} based on equation (19), whose calibration results are listed in Table 1.

V. DISCUSSION

A. SHEAR STRAIN SENSING MODEL

Initially, in the shear strain sensing model, the piezoelectric charge was modeled by the bending and stretching motions

TABLE 1. Calibration result of the shear stress measurement.

Measured height (mm)	0.5	2.5	4.5	6.5	8.5	10.5
Composite shear modulus $G_{com}(10^5$ Pa)	27.55	2.97	2.14	2.40	2.17	3.38

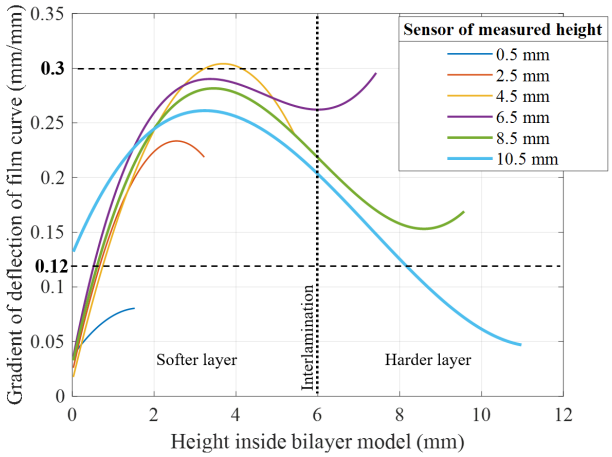

FIGURE 13. Gradient distribution of each film.

of the PVDF film sensor; however, as explained in the shear strain sensing model validation results in Section IV, the effect of the stretching model was relatively limited. From another point of view, because the stretching effect always generates a positive piezoelectric charge under both opposite shear states, a small q_s agrees with the fact that the output charge generation between the two opposite shear directions has high symmetry, as shown in Fig. 8. The limited effect of the stretching model can be explained by the small piezoelectric coefficient d_{31} by orders of magnitude.

In comparison, the bending model is sufficiently sensitive to represent the sensing mechanism. Therefore, for this type of piezoelectric film sensor, the effect of the deflection dominates the output signal. As derived in equation (5), the induced charge is directly related to the deflection differential of the free-end tip of the sensor film.

B. SHEAR STRAIN DISTRIBUTION

As plotted in Fig. 11, the measured shear strain distribution of the bilayer soft material in the depth direction first increases to a peak and then decreases. The measurement effect of substrate deformation reflected on the sensing element should be assessed. Here, the shear strain of the bilayer substrate in the experimental condition was calculated for comparison. According to the linear elasticity expressed in equation (18), when the surface displacement X is 2.5 mm, the shear strain γ_1 and γ_2 of each layer are 0.12 and 0.3, respectively [32]; however, the distribution measured by the sensor system in each layer shows a gradually varying value.

To describe the phenomenon intuitively, the gradient of the film deflection under the above-mentioned conditions is plotted in Fig. 13. The two horizontal dotted lines represent the actual shear strains γ_1 and γ_2 of the substrate. Sensor film

curves with different lengths were deformed in various ways. As flexible sensors, they are compliant with the deformation of the substrate, and the differential deflection approaches the linear shear strain of each layer; however, as mentioned in the stress sensing model, the stiffness of the built-in sensor is difficult to ignore. Sensor films with considerable stiffness, especially the shorter ones, tend to have a larger difference from the actual shear strain value.

C. LIMITATION AND FUTURE WORK

For strain measurement, the accuracy is limited by the stiffness of the embedded sensors and their arrangement relative to the substrate material. Direct measurement of the shear strain requires a more ideal flexible sensor, which is expected in material science. Furthermore, manufacture of the interposition system is also difficult. If a very light and soft sensor is applied, a manufacturing operation is required to cautiously construct the soft PVDF film in a flat state. As applied in this study, a type of urethane resin is recommended as the substrate soft material, which can solidify from the liquid state without influencing the natural state of the sensor.

Based on the above discussions, this sensor system can be applied to various materials for sensitive measurement of both the shear strain and shear stress. To simulate human experimentation, anthropometric dummies or substitute animal tissue are often applied. This sensor system can render the biomaterials smarter and provide more information on the internal physical phenomena. In future, human-body dummy models equipped with the built-in sensor system will be developed and used for conducting human contact safety experiments.

VI. CONCLUSION

For the internal physical measurement of soft materials, a sensor system was developed in this study to measure the internal shear strain and stress distribution of bilayer artificial skin, using built-in flexible PVDF films. To explain the sensing mechanism, sensing models were mathematically established based on piezoelectricity and material mechanics. The shear strain sensing model considers the bending and stretching motions of the film sensor. The shear stress sensing model proposes a definition of the shear modulus for composite material.

In the validation experiment, the shear strain and stress of the bilayer artificial skin substrate in the depth direction were measured. The deflection of the embedded PVDF films was captured by a video camera and digitized through image processing. Excellent agreement of the charge generation results between the model and measurement was found with a high R^2 coefficient of determination of 0.974. In addition, calibration for both strain and stress measurements was introduced. The measured shear strain distribution tendency indicated the boundary of the multimaterial and provided a reasonable mechanical explanation. Adaptable suggestions on improving the measurement and manufacturing accuracy were additionally provided.

In summary, the application of the proposed sensor system for internal shear strain and stress sensing in soft materials was systematically validated. This sensor system is expected to have immense potential for application in soft material measurement and soft robotics development.

REFERENCES

[1] S. Xu, D. M. Vogt, W.-H. Hsu, J. Osborne, T. Walsh, J. R. Foster, S. K. Sullivan, V. C. Smith, A. W. Rousing, E. C. Goldfield, and R. J. Wood, "Biocompatible soft fluidic strain and force sensors for wearable devices," *Adv. Funct. Mater.*, vol. 29, no. 7, Feb. 2019, Art. no. 1807058.

[2] L. Viry, A. Levi, M. Totaro, A. Mondini, V. Mattoli, B. Mazzolai, and L. Beccai, "Flexible three-axial force sensor for soft and highly sensitive artificial touch," *Adv. Mater.*, vol. 26, no. 17, pp. 2659–2664, 2014.

[3] Y.-L. Park, B.-R. Chen, N. O. Pérez-Arancibia, D. Young, L. Stirling, R. J. Wood, E. C. Goldfield, and R. Nagpal, "Design and control of a bio-inspired soft wearable robotic device for ankle–foot rehabilitation," *Bioinspiration Biomimetics*, vol. 9, no. 1, 2014, Art. no. 016007.

[4] A. Miriyev, K. Stack, and H. Lipson, "Soft material for soft actuators," *Nature Commun.*, vol. 8, no. 1, pp. 1–8, Dec. 2017.

[5] Z. T. H. Tse, Y. Chen, S. Hovet, H. Ren, K. Cleary, S. Xu, B. Wood, and R. Monfaredi, "Soft robotics in medical applications," *J. Med. Robot. Res.*, vol. 3, nos. 3–4, Sep. 2018, Art. no. 1841006.

[6] J. C. Yeo, J. Yu, Z. M. Koh, Z. Wang, and C.-T. Lim, "Wearable tactile sensor based on flexible microfluidics," *Lab Chip*, vol. 16, no. 17, pp. 3244–3250, 2016.

[7] M. Kaltenbrunner T. Sekitani, J. Reeder, T. Yokota, K. Kuribara, T. Tokuhara, M. Drack, R. Schwödiauer, I. Graz, S. Bauer-Gogonea, S. Bauer and T. Someya, "An ultra-lightweight design for imperceptible plastic electronics," *Nature*, vol. 499, no. 7459, pp. 458–463, Jul. 2013.

[8] B. Bonfiglioli and G. Pascale, "Internal strain measurements in concrete elements by fiber optic sensors," *J. Mater. Civil Eng.*, vol. 15, no. 2, pp. 125–133, Apr. 2003.

[9] K. Holst, H. Liebgott, J. E. Wilhjelm, S. Nikolov, S. T. Torp-Pedersen, P. Delachartre, and J. A. Jensen, "Internal strain estimation for quantification of human heel pad elastic modulus: A phantom study," *Ultrasonics*, vol. 53, no. 2, pp. 439–446, Feb. 2013.

[10] A. I. Bowler, B. W. Drinkwater, and P. D. Wilcox, "An investigation into the feasibility of internal strain measurement in solids by correlation of ultrasonic images," *Proc. Roy. Soc. A, Math., Phys. Eng. Sci.*, vol. 467, no. 2132, pp. 2247–2270, Aug. 2011.

[11] A. Takahashi, S. Suzuki, Y. Aoyama, M. Umezu, and K. Iwasaki, "A three-dimensional strain measurement method in elastic transparent materials using tomographic particle image velocimetry," *PLoS ONE*, vol. 12, no. 9, Sep. 2017, Art. no. e0184782.

[12] B. Shih, D. Shah, J. Li, T. G. Thuruthel, Y.-L. Park, F. Iida, Z. Bao, R. Kramer-Bottiglio, and M. T. Tolley, "Electronic skins and machine learning for intelligent soft robots," *Sci. Robot.*, vol. 41, 2020, Art. no. eaaz9239.

[13] C. Majidi, "Artificial skin," *Mech. Eng.*, vol. 138, no. 3, pp. S17–S21, 2016.

[14] R. Dahiya, N. Yogeswaran, F. Liu, L. Manjakkal, E. Burdet, V. Hayward, and H. Jorntell, "Large-area soft e-skin: The challenges beyond sensor designs," *Proc. IEEE*, vol. 107, no. 10, pp. 2016–2033, Oct. 2019.

[15] K. Noda, K. Hoshino, K. Matsumoto, and I. Shimoyama, "A shear stress sensor for tactile sensing with the piezoresistive cantilever standing in elastic material," *Sens. Actuators A, Phys.*, vol. 127, no. 2, pp. 295–301, Mar. 2006.

[16] H. Joodaki and M. B. Panzer, "Skin mechanical properties and modeling: A review," *Proc. Inst. Mech. Eng., H, J. Eng. Med.*, vol. 232, no. 4, pp. 323–343, Apr. 2018.

[17] Y. Iki, Y. Yamada, Y. Akiyama, S. Okamoto, and J. Liu, "Designing a dummy skin by evaluating contacts between a human hand and a robot end tip," in *Proc. IEEE/RSJ Int. Conf. Intell. Robots Syst. (IROS)*, Oct. 2020, pp. 11337–11344.

[18] T.-D. Ngo, "Introduction to composite materials," in *Composite and Nanocomposite Materials*, T.-D. Ngo, Ed. Rijeka, Croatia: IntechOpen, 2020, ch. 1, doi: 10.5772/intechopen.91285.

[19] C. Abeykoon, "Design and applications of soft sensors in polymer processing: A review," *IEEE Sensors J.*, vol. 19, no. 8, pp. 2801–2813, Apr. 2019.

[20] F. Li, Y. Akiyama, X. Wan, S. Okamoto, and Y. Yamada, "Measurement of shear strain field in a soft material using a sensor system consisting of distributed piezoelectric polymer film," *Sensors*, vol. 20, no. 12, p. 3484, Jun. 2020.
[21] F. Li, Y. Akiyama, X. Wan, Y. Yamada, and S. Okamoto, "Shear stress sensor for soft material with built-in piezoelectric polymer films," in *Proc. IEEE 8th Global Conf. Consum. Electron. (GCCE)*, Oct. 2019, pp. 656–658.
[22] H. Kawai, "The piezoelectricity of poly (vinylidene fluoride)," *Jpn. J. Appl. Phys.*, vol. 8, no. 7, p. 975, 1969.
[23] S. D. Mahapatra, P. C. Mohapatra, A. I. Aria, G. Christie, Y. K. Mishra, S. Hofmann, and V. K. Thakur, "Piezoelectric materials for energy harvesting and sensing applications: Roadmap for future smart materials," *Adv. Sci.*, vol. 8, no. 17, Sep. 2021, Art. no. 2100864.
[24] A. V. Shirinov and W. K. Schomburg, "Pressure sensor from a PVDF film," *Sens. Actuators A, Phys.*, vol. 142, no. 1, pp. 48–55, 2008.
[25] H. Lee, R. Cooper, B. Mika, D. Clayton, R. Garg, J. M. Gonzalez, S. B. Vinson, S. Khatri, and H. Liang, "Polymeric sensors to monitor cockroach locomotion," *IEEE Sensors J.*, vol. 7, no. 12, pp. 1698–1702, Dec. 2007.
[26] M. Luo, D. Liu, and H. Luo, "Real-time deflection monitoring for milling of a thin-walled workpiece by using PVDF thin-film sensors with a cantilevered beam as a case study," *Sensors*, vol. 16, no. 9, p. 1470, Sep. 2016.
[27] B. Choi, H. Ryeol Choi, and S. Kang, "Development of tactile sensor for detecting contact force and slip," in *Proc. IEEE/RSJ Int. Conf. Intell. Robots Syst.*, Aug. 2005, pp. 2638–2643.
[28] J. Sirohi and I. Chopra, "Fundamental understanding of piezoelectric strain sensors," *J. Intell. Mater. Syst. Struct.*, vol. 11, no. 4, pp. 246–257, Apr. 2000.
[29] F. P. Beer, R. Johnston, J. Dewolf, and D. Mazurek, *Mechanics of Materials*. New York, NY, USA: McGraw-Hill, 1981, pp. 150–233.
[30] P. A. Hassan, G. Verma, and R. Ganguly, "Soft materials-properties and applications," in *Functional Materials: Preparation, Processing and Applications*. Amsterdam, The Netherlands: Elsevier, 2011, p. 1.
[31] Y. Akiyama, Y. Yamada, K. Ito, S. Oda, S. Okamoto, and S. Hara, "Test method for contact safety assessment of a wearable robot -analysis of load caused by a misalignment of the knee joint," in *Proc. IEEE RO-MAN: 21st IEEE Int. Symp. Robot Hum. Interact. Commun.*, Sep. 2012, pp. 539–544.
[32] K. L. Johnson and K. L. Johnson, *Contact Mechanics*. Cambridge, U.K.: Cambridge Univ. Press, 1987.

FENGYU LI was born in Qingdao, Shandong, China, in 1994. She received the B.S. degree in engineering from Wuhan University, Hubei, China, in 2016, and the M.S. degree in engineering from Nagoya University, Nagoya, Japan, in 2020.

YASUHIRO AKIYAMA (Member, IEEE) received the B.E. degree in engineering from the Tokyo Institute of Technology, Tokyo, Japan, in 2006, and the M.S. and Ph.D. degrees in engineering from The University of Tokyo, Tokyo, in 2008 and 2011, respectively. Since 2016, he has been an Assistant Professor with Nagoya University, Japan. His main research interests include mechanical safety, human–robot interaction, and biomechanics.

XIANGLONG WAN (Member, IEEE) received the Ph.D. degree in engineering from Kobe University, Japan. He is currently a Lecturer at the School of Automation and Electrical Engineering, University of Science and Technology Beijing, China. His main research interests include singular configuration in robotics, rehabilitation robots, gait analysis, and biomechanics.

SHOGO OKAMOTO (Member, IEEE) received the Ph.D. degree in information sciences from Tohoku University, in 2010. From 2010 to 2021, he was with Nagoya University. He is currently an Associate Professor with the Department of Computer Science, Tokyo Metropolitan University. His research interests include haptics, assistive robotics, human-centered informatics, and affective engineering.

YOJI YAMADA (Member, IEEE) received the Ph.D. degree from the Tokyo Institute of Technology. Since 1983, he has been with the Toyota Technological Institute, Nagoya, Japan. In 2004, he joined the Safety Intelligence Research Group, National Institute of Advanced Industrial Science and Technology (AIST), as a Leader. In 2009, he joined the Department of Mechanical Science and Engineering, Graduate School of Engineering, Nagoya University, as a Professor.